Supporting Information

Biomimetic brain-like nanostructures for solid polymer electrolytes with fast ion transport.

Ahmed Eissa Abdelmaoula,[1,3] Lulu Du,[1] Lin Xu,[1,2*] Yu Cheng,[1] Amir A. Mahdy,[3] Muhammad Tahir,[1] Ziang Liu,[1] and Liqiang Mai, [1,2*]

[1] State Key Laboratory of Advanced Technology for Materials Synthesis and Processing, School of Materials Science and Engineering, Wuhan University of Technology, Wuhan 430070, China.

[2] Foshan Xianhu Laboratory of the Advanced Energy Science and Technology Guangdong Laboratory, Xianhu Hydrogen Valley, Foshan 528200, China.

[3] Mining and Metallurgical Department, Faculty of Engineering, Al-Azhar University, Cairo 11884, Egypt.

* Corresponding authors emails: linxu@whut.edu.cn; mlq518@whut.edu.cn

SUPPLEMENTARY FIGURES

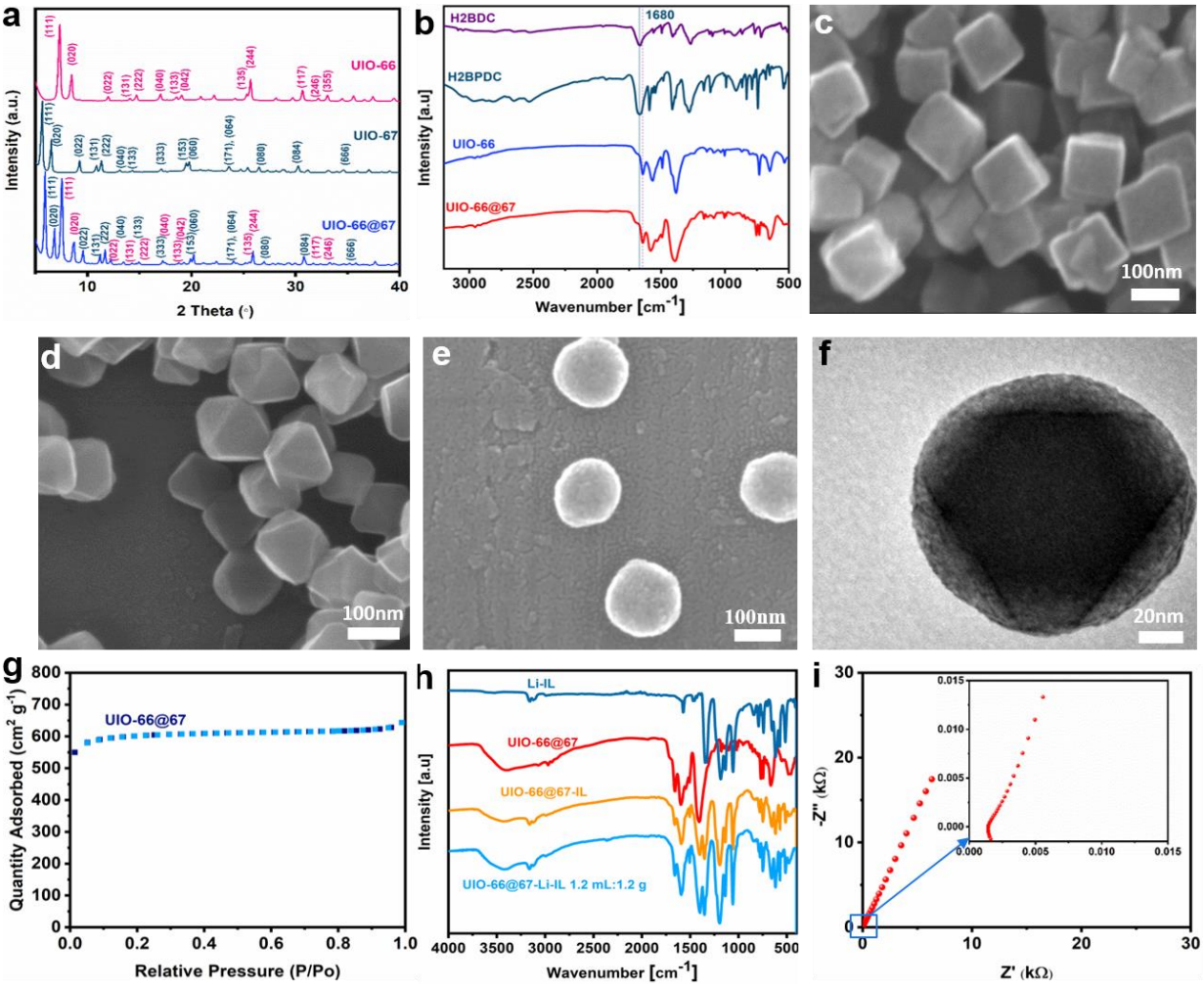

Figure S1 (a) X-ray diffraction patterns of the as-prepared UIO-66, UIO-67 and UIO-66@67. (b) FT-IR characterization of BDC, BPDC, UIO-66 and UIO-66@67. (c) SEM image of UIO-66. (d) SEM image of UIO-67. (e) SEM image of UIO-66@67. (f) TEM image of UIO-66@67. (g) N2 adsorption/desorption isothermal linear plots of UIO-66@67 and UIO-66@67-IL. (h) FT-IR spectra of UIO-66@67-IL with 1.2ml Li-IL amount, core-shell with ionic liquid, pristine Li-IL and pristine UIO-66@67. (i) AC impedance spectra of UIO-66@67-IL solid electrolyte with 1.2 g UIO66@67 to 1.2 ml Li-IL composition.

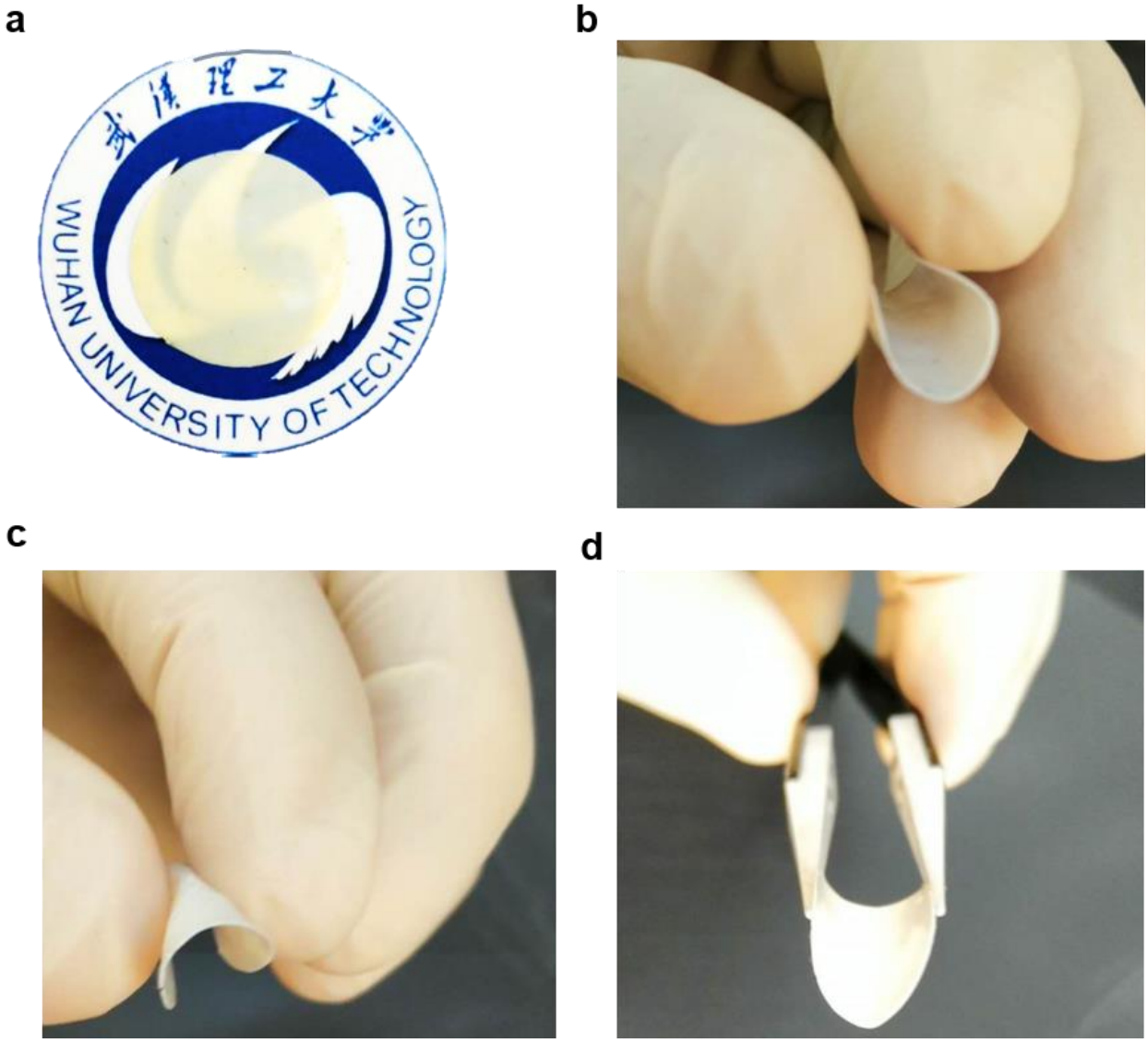

Figure S2 (a, b, c, d) Photographs of the free-standing, flexible BBLNs solid polymer electrolyte with 40% UIO-66@67-IL fillers.

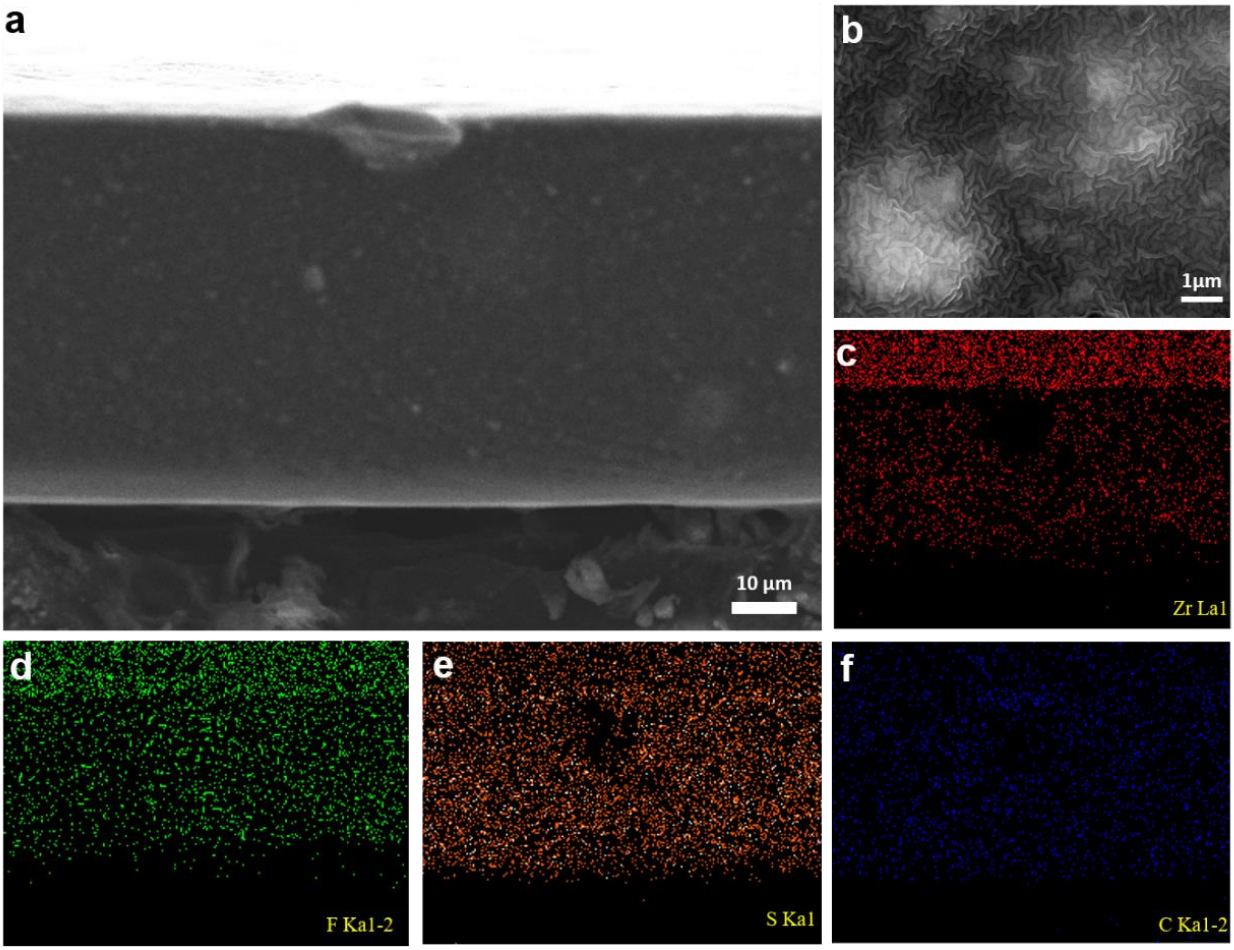

Figure S3 Structure characterization of BBLNs solid polymer electrolyte. (a, b) cross section with deferent magnification and (c, d, e, f) Zr, F, S, C elemental mapping.

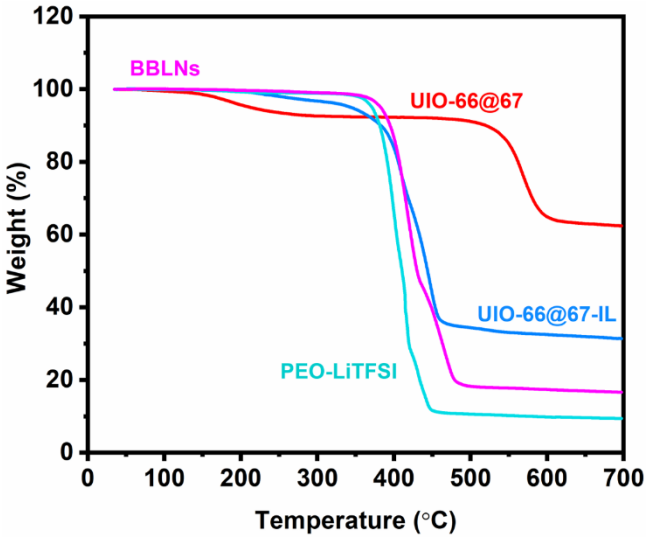

Figure S4 Thermal gravimetric analysis curve of UIO-66@67, PEO-LiTFSI, UIO-66@67-IL and BBLNs solid polymer electrolyte.

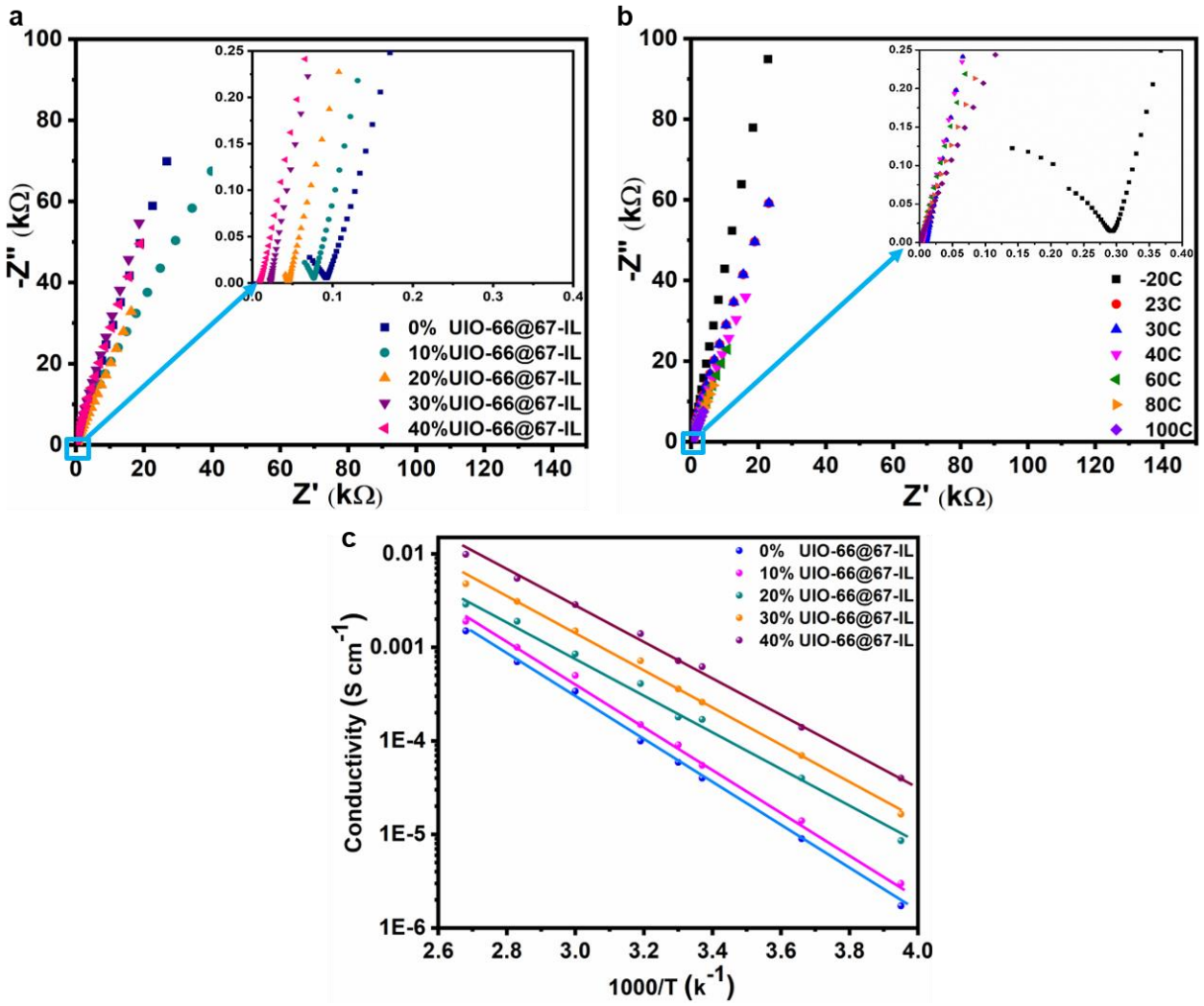

Figure S5 (a) EIS of BBLNs solid polymer electrolyte with different composition at room temperature. (b) Arrhenius plots of BBLNs solid polymer electrolyte with 40% UIO-66@67-IL at different temperature, (c) Arrhenius plots of BBLNs solid polymer electrolyte with different compositions at different temperatures.

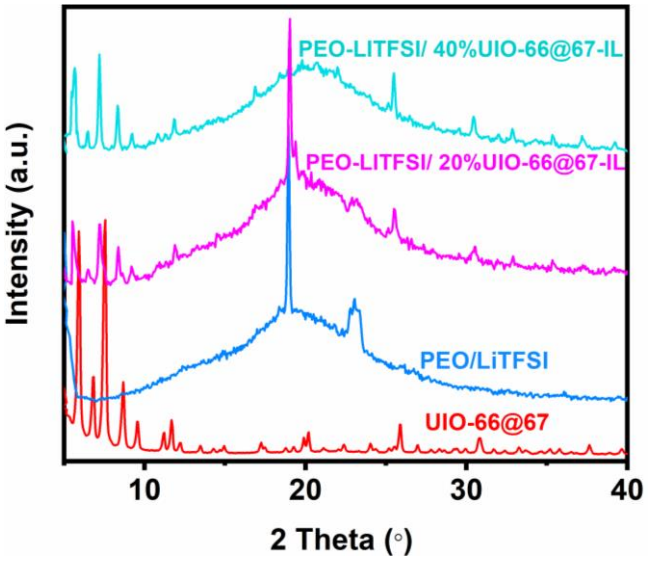

Figure S6 XRD patterns of PEO-LiTFSI, UIO-666@67, PEO-LiTFSI/ 20% UIO-66@67-IL and PEO-LiTFSI/ 40% UIO-66@67-IL.

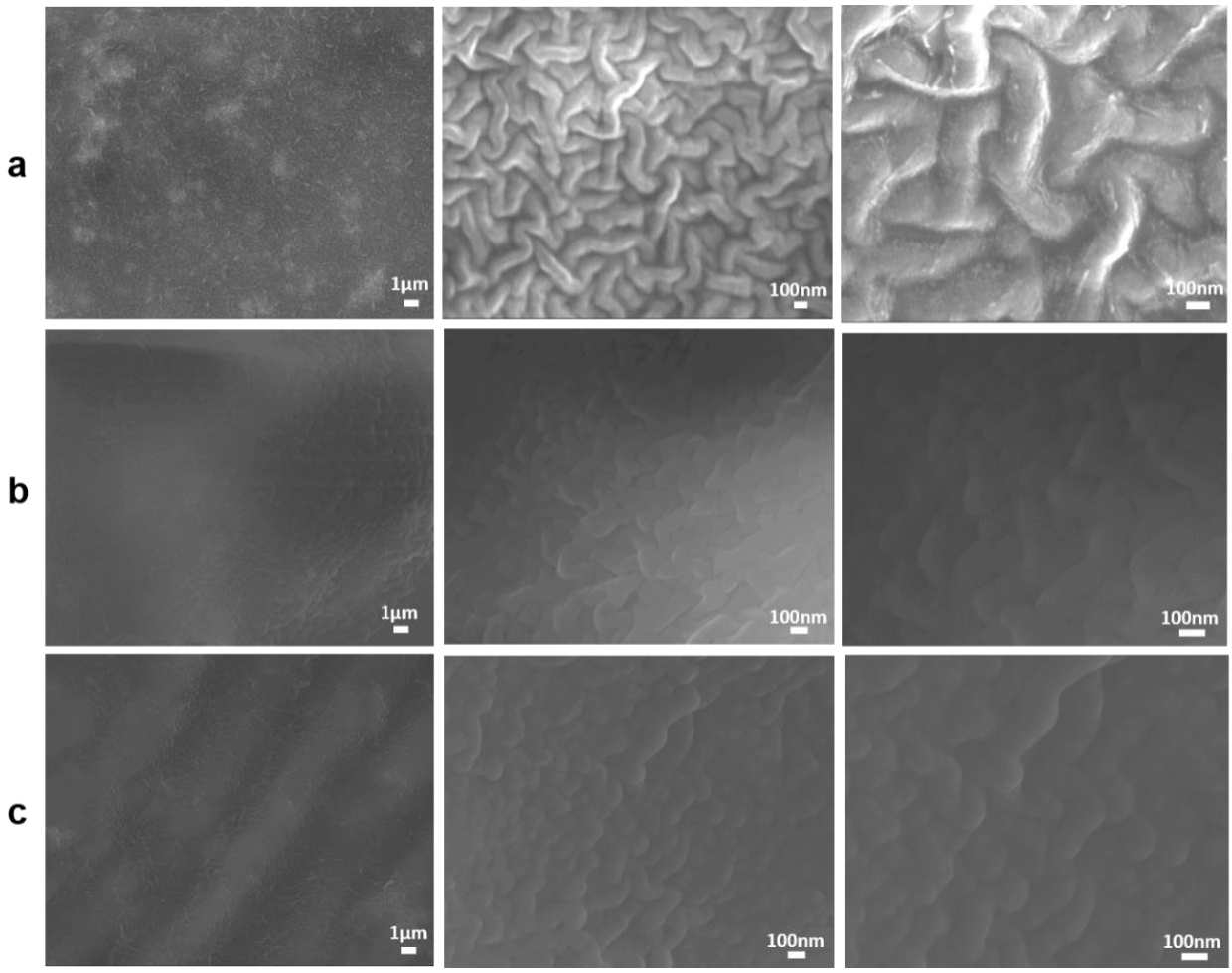

Figure S7 Morphology characterization of PEO-LiTFSI/UIO-Li-IL fillers. (a) SEM images of BBLNs solid polymer electrolyte with different magnifications. (b) SEM images of PEO-LiTFSI/UIO-66-IL solid electrolyte with different magnifications. (c) SEM images of PEO-LiTFSI/UIO-67-IL solid electrolyte with different magnifications.

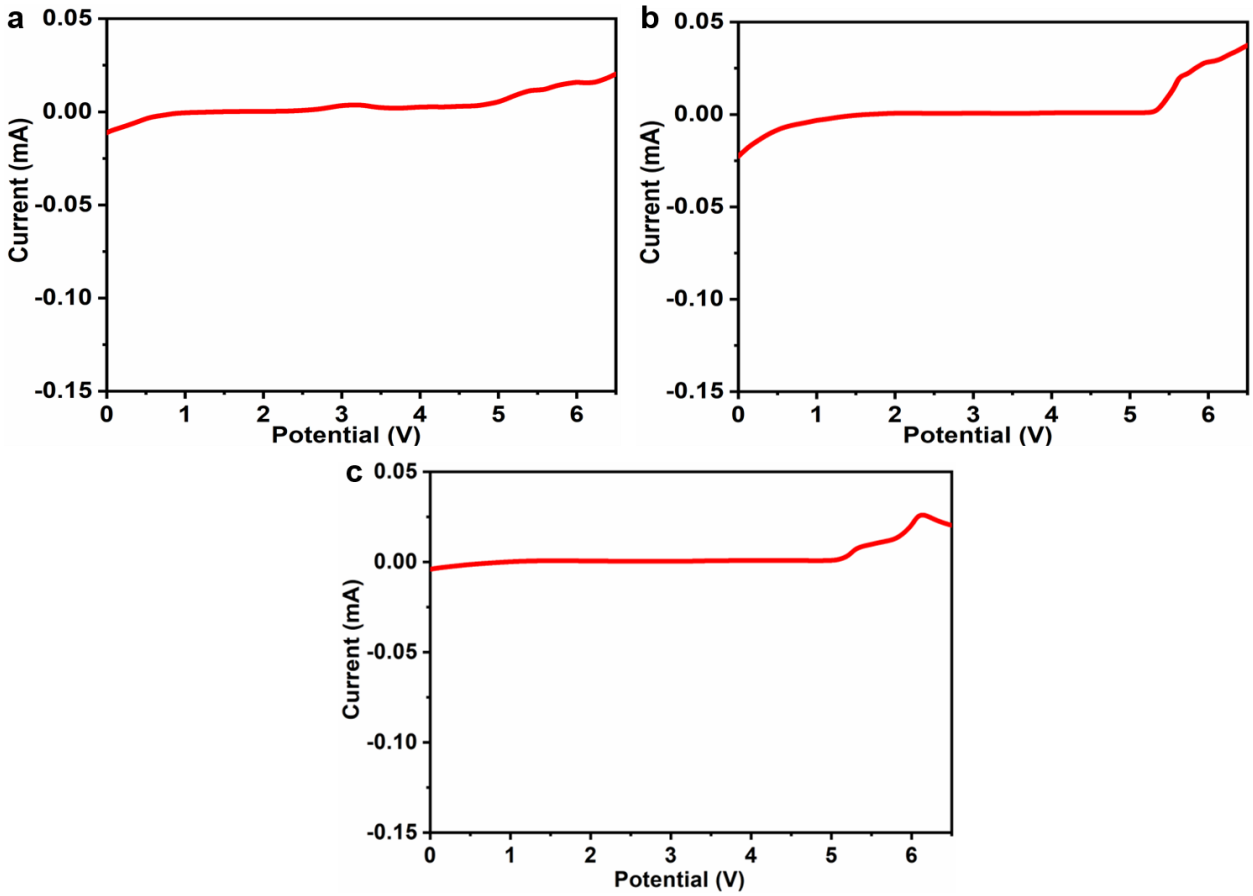

Figure S8 Linear sweep voltammogram of (a) PEO-LiTFSI/UIO-66-IL, (b) PEO-LiTFSI/UIO-67-IL and (c) BBLNs solid polymer electrolytes at scan rate of 0.5mV and 25 ˚C.

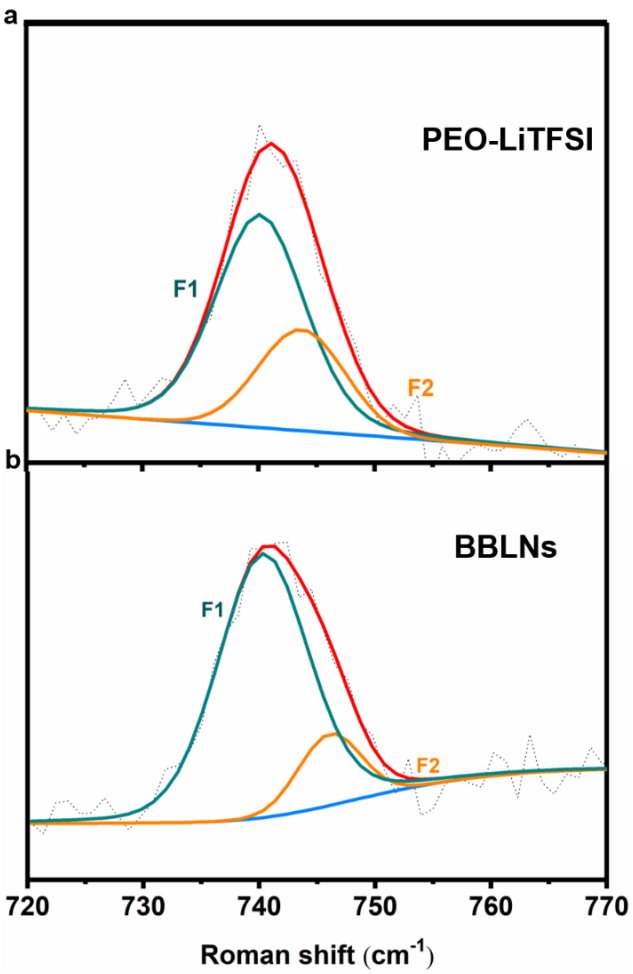

Figure S9 Raman spectra of the (a) BBLNs solid polymer electrolyte and (b) PEO-LiTFSI fitted with F1 and F2 band.

Fitted Lorentzian profiles at 743 cm−1 (F1) and 747 cm−1 (F2), are used to calculate the free TFSI- and the ion cluster [Li(TFSI)2-], respectively by the following equation.1-3

$$free\ TFSI-= \frac{AF1}{A_{F1}+A_{F2}} \text{ X } 100\% \qquad (1)$$

Where AF1 and AF2 are corresponding to the integrated intensity of the F1 and F2 band.

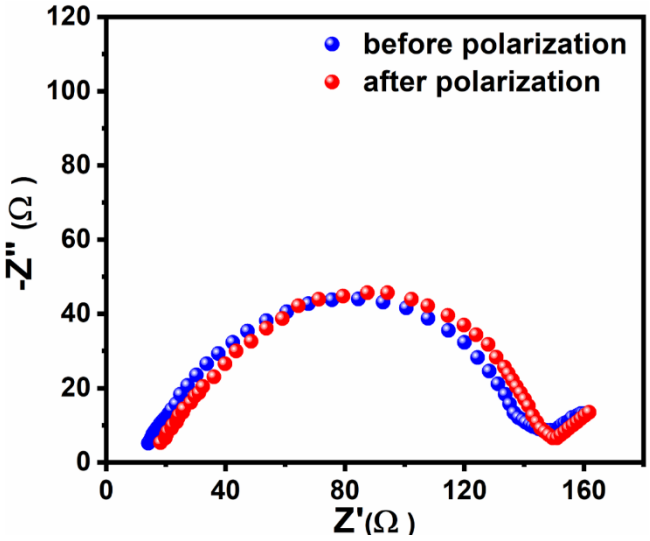

Figure S10. AC impedance spectra of BBLNs before and after the galvanostatic cycling at 200 μA cm^{-2} and room temperature.

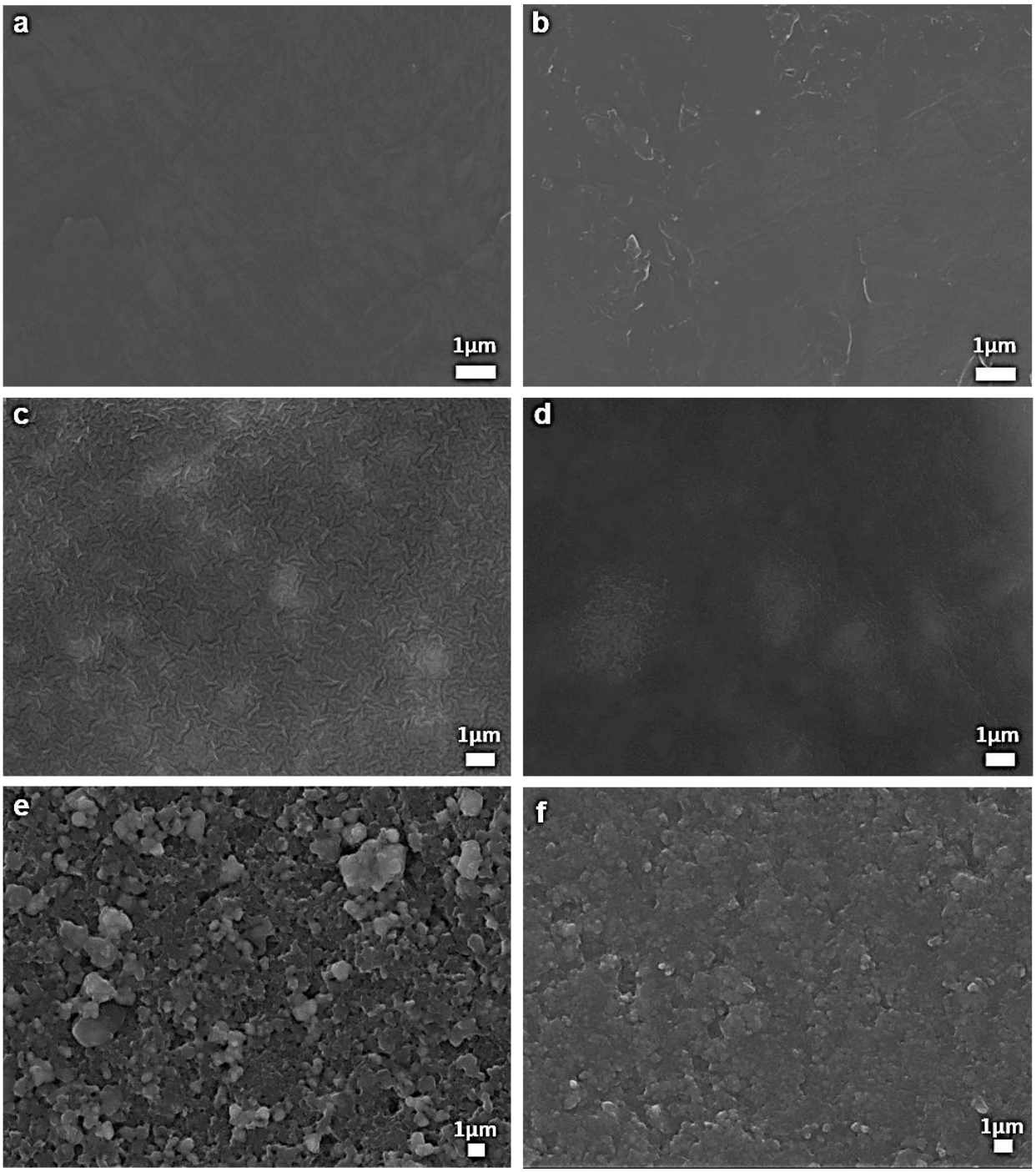

Figure S11 Surface morphology SEM images before and after cycling of (a, b) Li metal anode, (c, d) BBLNs solid polymer electrolyte, and (e, f) LFP electrode before and after charge /discharge cycling.

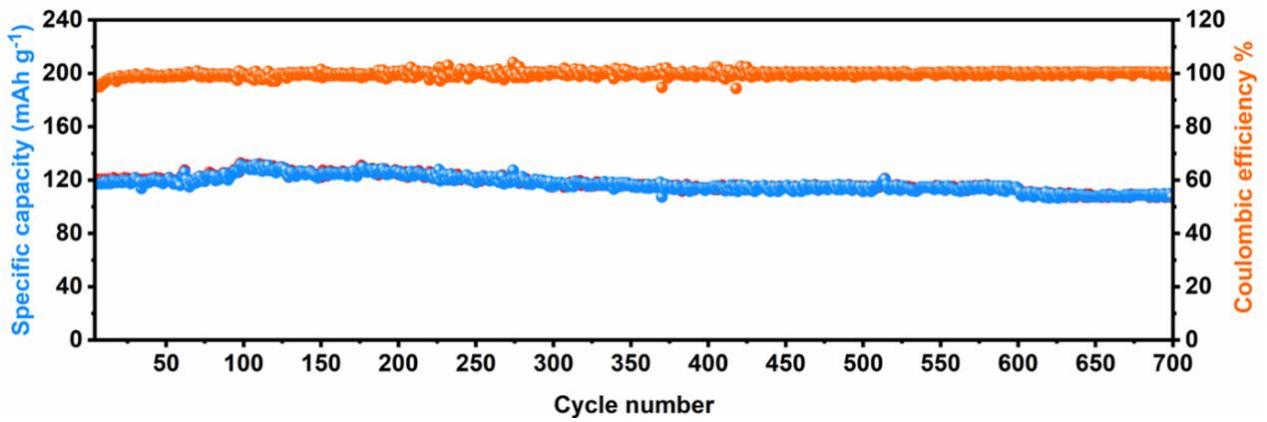

Figure S12 Cycling performance of Li/BBLNs/LFP cells with 40% batteries fillers at 3 C and room temperature.

Table S1 Comparison for ionic conductivity and Li+ transference number of CTN solid polymer electrolyte and other solid electrolytes.

Type of electrolyte	σ (S cm^{-1})	t_{Li}^+	Ref.
PEO@CMOF	6×10^{-4} (60 ˚C)	0.72 (27 ˚C)	4
HSPE	4.3×10^{-4} (30 ˚C)		5
PEO-n-UIO-66	1.3×10^{-4} (30 ˚C)	0.35 (27 ˚C)	6
LLZO-UIO-67(Zr)	1×10^{-4} (25 ˚C)	0.18	7
C-CSE	4.26×10^{-4} (30 ˚C)	0.67 (30 ˚C)	8
SPE2-PI-ZIF8	4.7×10^{-4} (27 ˚C)	0.68 (27 ˚C)	9
MOF+PC[$Cu_4(ttpm)_2(CuCl2)_{0.6}(LiBr)_{1.8}$]	3.2×10^{-5} (25 ˚C)	0.42	10
UIO-67-PC	6.5×10^{-4} (25 ˚C)	0.65	11
MCM-41-IL	3.98×10^{-4} (30 ˚C)	0.17	12
BBLNs	9.2×10^{-4} (25 ˚C)	0.74 (25 ˚C)	Current work

Table S2 Comparison for electrochemical performance of CTN solid polymer electrolyte and other solid electrolytes.

Type of electrolyte	Lithium compatibility	Capacity mAh g^{-1}/No. of cycles, retention	Cathode composition/ loading amount	Ref.
PEO@CMOF	200 cycles at 500 μA cm^{-2} and 60 ˚C	110/300, retention 85 % at 1C and 60 ˚C	50% LFP, 10% acetylene black, 30% LiTFSI, and 10% PEO / 2 mg cm^{-2}	4
HSPE		153/40, retention 100 % at 0.5C and 60 ˚C	LFP, super P, and PVDF (7:2:1)	5
PEO-n-UIO-66	500 cycles at 500 μA cm^{-2} and 60 ˚C	157/100, retention 91.7 % at 0.5C and 27 ˚C	LFP, UIO-Li-IL, Ketjen black (4:4:2)/ 1-2 mg	6
PEO/LITFSI + LLZO nanowires	1075 cycles at 1000 μA cm^{-2} and 60 ˚C	158/80, retention 92 % at 0.1C and 45 ˚C	LFP, PEO/LiTFSI, carbon black (8:1:1)/ 1.8 mg cm^{-2}	7
C-CSE	1040 cycles at 100 μA cm^{-2} and 25 ˚C	130/120, retention 76.8 % at 0.1C and 25 ˚C	commercial LFP / 8 mg	8
SPE2-PI-ZIF8	800 cycles at 100 μA cm^{-2} and 60 ˚C	115/300, retention 73 % at 0.1C and 25 ˚C	LFP, super P, PVdF (8:1:1) / 4-5 mg cm^{-2}	9
MIL-101(Cr)-DETA-Li	700 cycles at 200 μA cm^{-2} and 30 ˚C	153/50, retention 100 % at 0.2C and 27 ˚C	LFP, super P, PVdF (8:1:1) / 2-3 mg cm^{-2}	13
BBLNs	6500 cycles at 400 μA cm^{-2} and 25 ˚C	155/200, retention 99 % at 0.2C and 25 ˚C	LFP, acetylene black, UIO-66@67-IL (5:2:5) / 4 mg cm^{-2}	**Current work**

REFERENCES

1 Borodin O, Smith GD. LiTFSI Structure and Transport in Ethylene Carbonate from Molecular Dynamics Simulations. J. Phys. Chem. B 2006, 110: 4971-4977.

2 Duluard S, Grondin J, Bruneel JL, et al. Lithium Solvation and Diffusion in the 1-Butyl-3-Methylimidazolium Bis(Trifluoromethanesulfonyl)Imide Ionic Liquid. J. of Raman Spectroscopy 2008, 39: 627-632.

3 Huang J, Hollenkamp AF. Thermal Behaviour of Ionic Liquids Containing the FSI Anion and the Li^+ Cation. J. Phys. Chem. C 2010, 114: 21840-21847.

4 Huo H, Wu B, Zhang T, et al. Anion-Immobilized Polymer Electrolyte Achieved by Cationic Metal-Organic Framework Filler for Dendrite-Free Solid-State Batteries. Energy Storage Materials 2019, 18: 59.

5 Wang Z, Wang Z, Yang L, et al. Boosting Interfacial Li^+ Transport with A MOF-Based Ionic Conductor for Solid-State Batteries. Nano Energy 2018, 49: 580-587.

6 Wu JF, Guo X. MOF-Derived Nanoporous Multifunctional Fillers Enhancing the Performances of Polymer Electrolytes for Solid-State Lithium Batteries. J. Mater. Chem. A 2019, 7: 2653-2659.

7 Wan Z, Lei D, Yang W, et al. Low Resistance–Integrated All-Solid-State Battery Achieved by $Li_7La_3Zr_2O_{12}$ Nanowire Upgrading Polyethylene Oxide (PEO) Composite Electrolyte and PEO Cathode Binder. Adv. Funct. Mater.2019, 29: 1805301.

8 Xia Y, Xu N, Du L, et al. Rational Design of Ion Transport Paths at The Interface of Metal-Organic Framework Modified Solid Electrolyte. ACS Appl. Mater. Interfaces 2020, 12: 22930-22938.

9 Wang G, He P, Fan LZ. Asymmetric Polymer Electrolyte Constructed by Metal–Organic Framework for Solid-State, Dendrite-Free Lithium Metal Battery. Adv. Funct. Mater. 2020, 31: 2007198.

10. Miner EM, Park SS, Dincă M. High Li^+ and $Mg2^+$ Conductivity in a Cu-Azolate Metal–Organic FrameworkJ. Am. Chem. Soc. 2019, 141: 4422.

11 Shen L, Wu HB, Liu F, et al. Creating Lithium-Ion Electrolytes with Biomimetic Ionic Channels in Metal–Organic Frameworks. Adv. Mater. 2018, 30: 1707476.

12 Han L, Wang Z, Kong D, et al. An Ordered Mesoporous Silica Framework Based Electrolyte with Nanowetted Interfaces for Solid-State Lithium Batteries. J. Mater. Chem. A 2018, 6: 21280-21286.

13 Li D, Wang J, Guo S, et al. Molecular-Scale Interface Engineering of Metal–Organic Frameworks toward Ion Transport Enables High-Performance Solid Lithium Metal Battery. Adv. Funct. Mater. 2020, 30: 2003945.